

Nanoscale

Accepted Manuscript



This is an *Accepted Manuscript*, which has been through the Royal Society of Chemistry peer review process and has been accepted for publication.

Accepted Manuscripts are published online shortly after acceptance, before technical editing, formatting and proof reading. Using this free service, authors can make their results available to the community, in citable form, before we publish the edited article. We will replace this *Accepted Manuscript* with the edited and formatted *Advance Article* as soon as it is available.

You can find more information about *Accepted Manuscripts* in the [Information for Authors](#).

Please note that technical editing may introduce minor changes to the text and/or graphics, which may alter content. The journal's standard [Terms & Conditions](#) and the [Ethical guidelines](#) still apply. In no event shall the Royal Society of Chemistry be held responsible for any errors or omissions in this *Accepted Manuscript* or any consequences arising from the use of any information it contains.



Raman Fingerprinting of Single Dielectric Nanoparticles in Plasmonic Nanopores

Sarp Kerman^{a,b}, Chang Chen^{a,b}, Yi Li^{b,c}, Wim Van Roy^a, Liesbet Lagae^{a,b}, Pol Van Dorpe^{a,b}

Received 00th January 20xx,
Accepted 00th January 20xx

DOI: 10.1039/x0xx00000x

www.rsc.org/

Plasmonic nano-apertures are commonly used for the detection of small particles such as nanoparticles and proteins by exploiting electrical and optical techniques. Plasmonic nanopores are metallic nano-apertures sitting on a thin membrane with a tiny hole. It has been shown that plasmonic nanopores with a given geometry identify internal molecules using Surface Enhanced Raman Spectroscopy (SERS). However, label-free identification of a single dielectric nanoparticle requires a highly localized field comparable to the size of the particle. Additionally, the particle's Brownian motion can jeopardize the amount of photons collected from a single particle. Here, we demonstrate that the combination of optical trapping and SERS can be used for the detection and identification of 20 nm polystyrene nanoparticles in plasmonic nanopores. This work is anticipated to contribute to the detection of small bioparticles, optical trapping and nanotribology studies.

Introduction

Plasmonic nano-apertures are proven to have several applications for the detection of molecules and nanoparticle by localizing both the optical field and fluidics in small volumes^{1–12}. There are a variety of optical detection techniques used with those structures. The most common is the red-shift in plasmon resonance of those nanostructures as molecules are bound inside¹¹. For fluorescence detection, the locally enhanced field is exploited to detect molecules and particles in small volumes¹². The optical trapping methods are also used to detect nanoparticles and proteins to investigate their kinetics^{1,7,9,10}. Plasmonic nanopores allow the use of more techniques to study the kinetics. They are metallic nano-apertures placed on a free standing membrane with a tiny hole^{3,11–22}. The kinetics of nanoparticles and molecules can be manipulated by applying electric potential across the nanopores^{3,11,12}. Plasmonic nanopores are mainly used for combining electrokinetic manipulation with optical detection techniques^{3,11–13}. Cecchini et al. have shown that tagged molecules on translocating metallic nanoparticles can be identified by Surface Enhanced Raman Spectroscopy (SERS) in

plasmonic nanopores³.

SERS stands out as an optical technique providing information about the vibrations of the molecules present in a thin (sub-nm) detection region and allows label-free identification. Several studies have shown that SERS allows the detection of single molecules^{4,23,24}. Although extensive work has been done on SERS detection of single molecules and single metallic nanoparticles^{3,4,23,25–27}, little research has been performed on the detection of single dielectric nanoparticle^{5,28,29}. Most biological nano-objects such as viruses, large proteins, small organelles etc. can fall under the category of dielectric nanoparticles. It is feasible to localize the optical field into a region (called 'hot spot') close to the size of the nanoparticle in order to detect and identify single particles with the use of SERS. However, $\sim\mu\text{s}$ diffusion time of nanoparticles through a plasmonic hot spot does not allow for the detection of the SERS signal produced by single particle due to the relatively long acquisition time required ($\sim\text{ms}$). By exploiting the strong gradient of the plasmonic field used for SERS, optical trapping can be used to keep the particle in the detection region¹. It is desirable to combine SERS with optical trapping for the detection and identification of single nanoparticles. SERS provides a new insight on optical trapping studies and gives the opportunity to observe the transient state of nanosized particles (damaged or undamaged) and may extend the optical trapping studies down to the molecular scale.

SERS detection attempts on individual nanoparticles performed to date have been mainly performed on metallic nanoparticles coated with molecular labels. The localized plasmonic field around the metallic particle is exploited for detection^{3,4,23,25–27}. There is limited research work on the identification of dielectric nano-particles and most of which

^a imec, Kapeldreef 75, Leuven, B3001, Belgium

^b Department of Physics and Astronomy, KU Leuven, Celestijnenlaan 200D, 3001 Leuven, Belgium

^c Department of Electrical Engineering, KU Leuven, Kasteelpark Arenberg 10, 3001 Leuven, Belgium

† Corresponding Author: Chang Chen, E-mail: chang.chen@imec.be

Electronic Supplementary Information (ESI) available: [Figure S1: The histogram of trapping event dwell times for different laser powers; Figure S2: The temperature distribution for the nanopore illuminated by 16 mW of 785 nm laser wavelength; Figure S3: The FDTD simulation results of the enhancement factor; Figure S4: The histogram of the peak positions of polystyrene nanoparticle in a different nanopore.]. See DOI: 10.1039/x0xx00000x

that is pertained to bio-particles such as viruses and proteins. SERS measurements of single polystyrene particles (100-1000 nm) and DPPC vesicle (1 μm) have been reported by using rough Ag surface^{28,29}. However, to identify particles even smaller than the diffraction limit, an efficient platform for subwavelength focusing is required. It is well known that the diffraction limit can be overcome by generating plasmons localized in a designated spot². In a gap-type plasmonic structure, the enhancement of the field increases for decreasing gap width. Nevertheless, the gap size is limited by the size of the nanoparticles. Therefore, the main challenge to design a platform for nanoparticle identification is having an efficiently enhanced localized spot with a size as small as the particle. Recently, Wheaton et al.⁵ presented their results on extraordinary acoustic Raman detection of single 20 nm polystyrene nanoparticles and globular proteins in double nanohole structures. The particles are trapped by the plasmonic field and small wavenumbers of Raman spectrum (0-5 cm^{-1}) are used to probe the low-frequency thermally driven motion of the nanoparticles. This range of the Raman spectrum gives information about the shape, size and mechanical properties of the particle. However, a feasible method used to identify the particle can rely on the molecular vibrations modes of Raman spectroscopy. The 'fingerprints' of molecules appear to be at higher wavenumbers (600-2000 cm^{-1}), which brings the need for more information particularly in this part of the spectrum to identify the nanoparticle.

SERS and Particle Trapping in Plasmonic Nanopores

Fig. 1 a shows the setup used to perform the SERS experiments. Fig. 1 b displays the state-of-art gold coated plasmonic nanopores⁶ which are shown to be capable of optically trapping 20 nm polystyrene beads⁷ and localizing the SERS detection region in small volumes with high enhancement⁸. Fig. 1 c depicts the intensity profile in those nanopores calculated by finite-difference time-domain (FDTD) simulation. In order to detect the SERS of a single 20 nm nanoparticle and benefit from optical trapping, we make use of this platform based on a single rectangular nanopore-cavity; rather than the aforementioned SERS measurements of dielectric nanoparticles, (e.g. Ag rough surface)^{28,29}.

Upon addition of the solution containing nanoparticles, a peak as shown in Fig. 1 d began flickering. The main difference with the other optical trapping experiments conducted before^{1,7,9,10} is here, we monitor the Raman spectrum changing in time. This brings more information about the state of the trapped nanoparticle; for instance, it makes it possible to monitor chemical changes in the nanoparticle such as photodegradation as plasmonic structures that have high enhancements may damage specimens and leave amorphous carbonaceous. Compared with other tracking methods developed for trapping studies, such as reflection/transmission spectroscopy or fluorescence, utilizing SERS is a straightforward method to monitor the surface molecules and molecular changes of nanoscaled trapped objects.

Using SERS to study optical trapping enlightens other questions such as what actually is being trapped. It was difficult to define the material being trapped by measuring the intensity of the light transmitted through the plasmonic

structure, which is currently the most common technique used for optical trapping of nanoparticles^{1,7,9,10}. By using Raman spectroscopy, different particles, or materials can be differentiated by their characteristic molecular vibrations. This analysis eliminates the question whether or not something other than the designated particle is affecting the platform. It is crucial for nanoparticle trapping platforms since they are highly vulnerable to contamination.

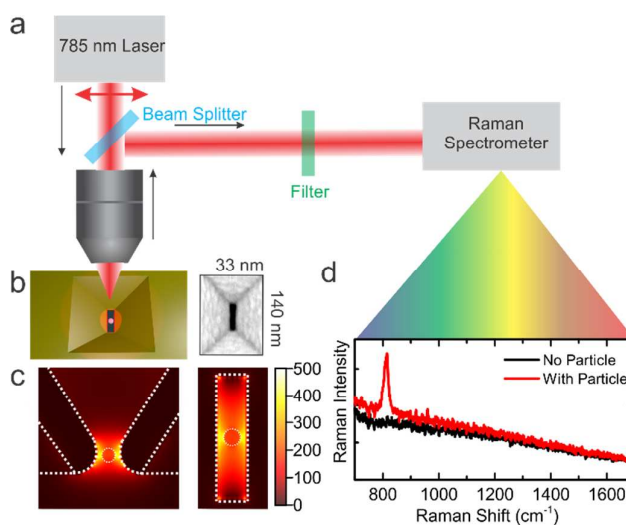


Fig. 1 Experimental setup and the study principles. (a) Schematics of Raman tweezer setup: a 785 nm laser, beam splitter, 60x (NA 0.9) water immersion objective, long-pass filter, Raman spectrometer (b) 3D representation and SEM image of the gold coated nanopore (c) FDTD simulation intensity profile of the nanopore (left - from the side, right - from the top) (d) Examples of Raman spectra with and without a 20 nm carboxyl modified polystyrene particle inside the nanopore.

Experimental Results and Discussion

SERS of 20 nm Polystyrene Nanoparticles

The Raman spectrum of polystyrene is long studied and well known. Raman spectroscopy provides information about the vibrations of molecules in bulk polystyrene. However, unlike Raman spectroscopy, SERS carries highly local information due to its fast decaying nature away from the metal surface³⁰. The properties at the interface of functionalized 20 nm polystyrene nanoparticles can be different than the bulk state. Therefore, it is necessary to look into the SERS of functionalized 20 nm polystyrene nanoparticles with different functionalization and compare those results with the bulk Raman spectrum of polystyrene particles.

Fig. 2 a shows the comparison of SERS spectra under three conditions: a single 20 nm polystyrene nanoparticle in a nanopore, a collection of the same nanoparticles in water on a rough gold surface and the bulk Raman spectrum of aggregated particles. Fig. 2 b shows the SERS spectra for

polystyrene nanoparticles with different molecular surface terminations. We first test nanoparticles with amidine and carboxyl modifications by using rough gold surfaces as the SERS substrates.

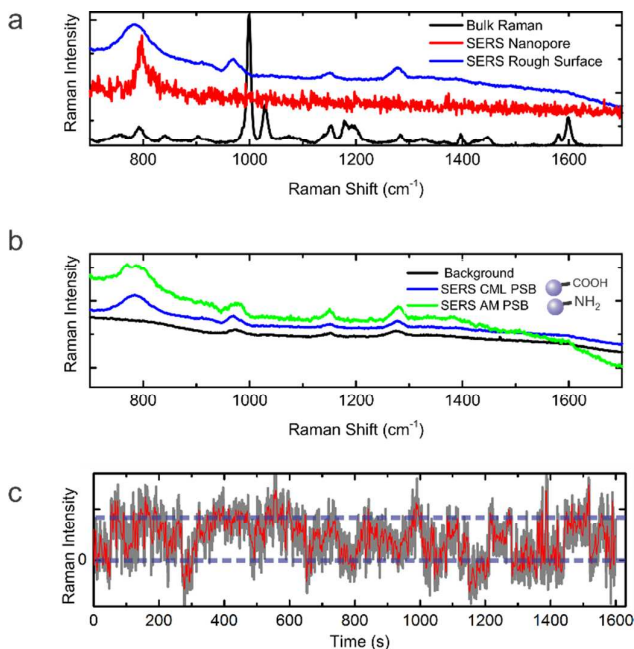


Fig. 2 Comparison between the Raman and SERS spectra of the nanoparticles and the SERS intensity fluctuation in the nanopore. (a) Comparison between the bulk Raman spectrum from the aggregation of nanoparticles, the SERS signal of a nanoparticle inside the nanopore, and the SERS of the nanoparticles on Au rough surface (b) The rough gold surface background, the SERS spectrum of amidine and carboxyl modified nanoparticles on the rough gold surface (c) The time series of the integrated SERS intensity of the peak at 785 cm⁻¹ inside the nanopore, the dashed lines indicate when there is no particle inside the nanopore and when the particle gives the maximum SERS intensity.

The amplitude of the SERS peaks and signal-to-noise ratio are not comparable between the different platforms presented here as the number of particles detected, integration time and the laser intensity used are different (see Methods). Therefore, we focus on the spectral differences.

The first thing that strikes our attention is that the strongest peak at 998 cm⁻¹ in the bulk Raman spectrum of polystyrene, assigned to the aromatic ring breathing mode³¹, is absent in the SERS spectra taken on both the rough surface and inside the nanopore (see Fig. 2 a). The only visible Raman peak in both SERS spectra is near 785 cm⁻¹, also appearing in the bulk Raman spectrum at 792 cm⁻¹, assigned to vibration of aromatic rings linked through gauche-gauche conformations of the aliphatic chain³¹.

Unfortunately, there is little existing literature on the SERS of polystyrene nanoparticles as small as 20 nm in the literature so far. For 100-1000 nm particles^{28,29} it is shown that the ring breathing mode can be observed. From the data reported it can be seen that there is a stable peak around 790 cm⁻¹.

Another report has compared the SERS signal from 200 and 20 nm polystyrene nanoparticles³². It can clearly be seen that the intensity of the ring breathing mode (at ~1000 cm⁻¹) is decreasing with the shrinking size of nanoparticles. Unfortunately, in that work, no spectral data below 900 cm⁻¹ is provided.

So far, the disappearance of the ring breathing mode peak at ~1000 cm⁻¹ is usually considered to be related to the flat orientation of phenyl rings to the metal surface^{33,34}. However, the reason is not fully understood as it is a nonpolarizable symmetrical vibrational mode³⁵, which should be enhanced independent of the molecular orientation. When the aromatic rings in polystyrene lie flat on the metal surface, it is shown that the peak around ~785 cm⁻¹ becomes stronger³⁶ as it is known to be a polarizable vibration peak³¹. However, the aromatic rings in polystyrene nanoparticles are completely randomly aligned, except at the interface of the particles. It has been shown that the organization of the water molecules at the polymer/water interface can orient the aromatic rings flat³⁷. This interpretation suggests that we mainly observe the nanoparticle/water interface in the SERS on both the rough gold surface and the nanopore. The localization of SERS on the surface of the nanoparticle can be explained by the fast decay of the electric field away from the metal surface³⁸ and the refractive index contrast between water ($n = 1.33$) and polystyrene ($n = 1.56$) (see Supporting Information S3). In the case of such highly heterogeneous electric field localization, it is also important to consider the gradient of electric field effect on SERS, which brings quadrupole-quadrupole and dipole-quadrupole contributions into the dipole-dipole contribution³⁹. Present literature has detailed the theoretical and experimental work carried out for benzene rings and proven that certain peaks may appear more prominently due to this effect⁴⁰.

The second observation made is that the functionalization of the particle is not detected by SERS. As shown in Fig. 2 b, the similar SERS spectra from different surface functionalized nanoparticles imply that the peak we observe at ~785 cm⁻¹ originates from polystyrene. The reason that only the polystyrene peak is observed can be due to the low surface coverage of the functional group.

The third point can be made by comparing the SERS spectrum from the nanopore and rough gold surface. The peak in the nanopore is considerably narrower when compared to the rough surface, suggests that a smaller amount of molecules were observed in nanopore⁴¹. This is expected because in the case of the rough surface we obtain the signal from many particles.

Fig. 2 c shows the fluctuation of the integrated SERS peak at 785 cm⁻¹ in the nanopore as a function of time. The stable appearance and disappearance of the peak and events of several seconds can be observed (see Supporting Information S1).

Temporal SERS and Trapping of 20 nm Nanoparticles in Nanopores

SERS and optical trapping experiments are performed on the carboxyl modified 20 nm polystyrene particles in the gold-coated nanopores. Fig. 3 shows the time dependence of the peak observed in the SERS spectrum. It can be observed that a stable peak appears for tens of seconds. 4 different laser powers are used to observe how the SERS peak and trapping stiffness are affected by the intensity. Although no sign of photodegradation is observed, a clear fluctuation in the SERS signal can be seen in Fig. 3 a. Besides the small fluctuations of $\sim 10 \text{ cm}^{-1}$, two different states of the SERS peak can be spotted, one at $\sim 785 \text{ cm}^{-1}$ and the other one at $\sim 815 \text{ cm}^{-1}$. A third state signifies the appearance of both peaks in the same spectrum, which rarely occurs ($\sim 4\%$ probability within Fig. 4 a). It should be noted that the peak at $\sim 785 \text{ cm}^{-1}$ is the expected peak according to the rough gold surface SERS measurements. Therefore, for further analysis the states observed are classified as “state 0” for when there is no peak, “state A” when the peak is around 785 cm^{-1} , “state B” when it’s around 815 cm^{-1} and “state M” when both peaks appear.

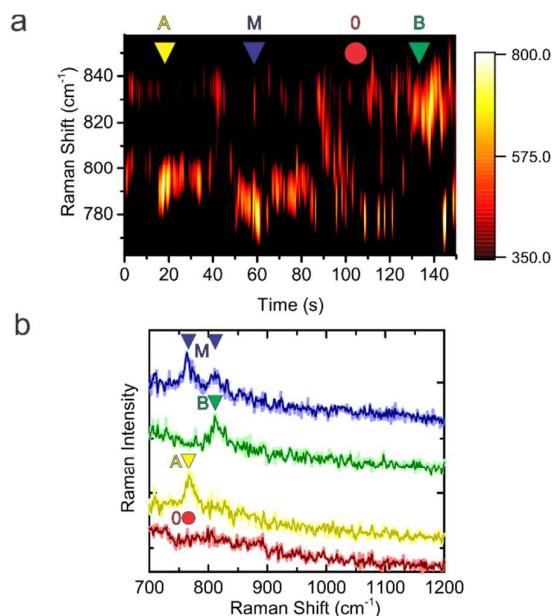


Fig. 3 Time series and SERS of a 20 nm polystyrene nanoparticle in the nanopore. (a) Waterfall plot of a trapped nanoparticle SERS in nanopore showing the temporal fluctuation of the peak position (b) The SERS of a single nanoparticle in different states.

To gain a better insight of the transitions between these states and their power dependence, we model the time-series data of peak positions as a Markov process. Fig. 4 a shows the probabilities of transitions from one state to another. It clearly shows that as the power increases, the transition probability from state 0 to A decreases while state 0 to B is not influenced by the power. Moreover, state A to 0 and state A to B transitions increase as the power increases, and state B to A transitions decrease while state B to 0 transitions seems to be

stable. All the probability analyses are performed on the data where state M does not occur.

From the power dependence of the probability of the transitions, it can be inferred that state A seems to lose its stability as the power increases; on the other hand, state B seems to be irresponsive to the power change.

Fig. 4 b displays multiple histograms of the peak positions for different laser powers. The instability of state A with the increasing power can also clearly be observed. The probability of the peak position being at state A decreases gradually as the laser power increases and state B increases.

The possible mechanism behind state A and state B

The possible reasons of the temporal changes in the Raman peak position are further elaborated and a model is sketched. Temporal shifts in the Raman spectrum are usually related to molecule tilting in single molecule Raman experiments^{41,42}. However, it is not plausible to assume that the observed SERS signal originates from a single molecule when nanoparticles are considered. Phase shifts can also explain the occurrence of temporal changes. Nevertheless, the glass transition temperature of polystyrene⁴³ ($\sim 100 \text{ }^\circ\text{C}$) is above the local temperature that is achieved with the highest laser power according to the simulations (see Supporting Information Figure S2), and this phase change does not cause a peak shift as has been observed⁴⁴.

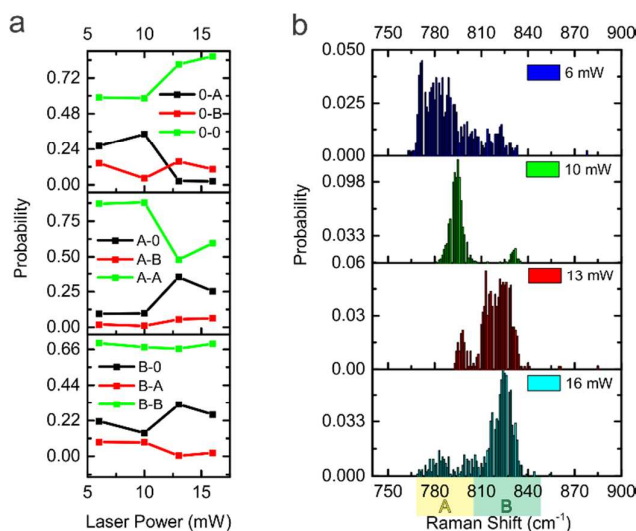


Fig. 4 Dynamics of SERS states in the nanopore by changing laser power. (a) Markov decision process probabilities for different laser powers for states 0, A and B (b) Histogram of SERS peak positions for 4 different laser powers, indicating the transition of Raman peak positions from 785 to 815 cm^{-1} .

Moreover, a phase change or chemical reaction would not cause smooth temporal shifts of peak position but rather end

up causing two discrete peak positions. One other possibility is a change in temperature depending on the particle's position inside the nanopore. However, since gold is a good thermal conductor, the temperature does not change significantly inside the detection area (see Supporting Information S2). Compressive stress on the molecules is known to increase the wavenumber of the Raman peaks⁴⁵. It is reported for polystyrene that under hydrostatic pressure⁴⁶, the peak at 785 cm^{-1} shifts approximately $4.6\text{ cm}^{-1}/\text{GPa}$. The nanoparticle inside the nanopore may undergo different stress states according to its position. In particular, a large change may be caused by contact pressure due to the adsorption of the particle. Since an increase in the wavenumber for state B compared to the expected peak position (state A) has been observed, it is proposed that state B represents the adsorbed state of the particle while state A represents the free state, i.e. where the particle is mostly moving inside the nanopore during one integration time. Fig. 5 depicts those 2 possible states. The probability of state A decreasing and state B increasing by increasing laser power also supports this hypothesis since increasing laser power also increases the temperature. At a higher temperature, it is conceivable that a free particle, in state A, would be more mobile than an adsorbed particle, in state B, and this particle can escape from the detection region. Referring back to the Markov's process, it has been observed that when the particle is adsorbed, its state is minimally affected by any laser power change while the chances of freely moving particle leaving the detection area increases with increasing laser power.

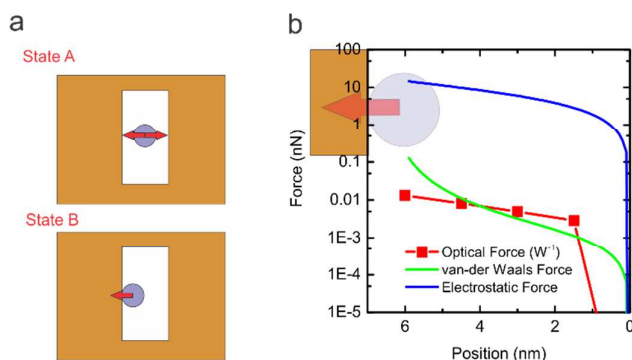


Fig. 5 Possible two states and the forces acting on the particle. (a) Representation of possible cases for state A, free, and state B, adsorbed state of nanoparticle (b) The forces acting on the particle inside the nanopore as it moves from one wall (6 nm) to the middle of the nanopore (0 nm)

To elaborate the adsorption of the nanoparticle to the nanopore's wall, the forces acting on the particle are calculated. The significant forces acting on the particle are van-der Waals force, electrostatic force due to image charge of the particle and optical force. Fig. 5 b shows those forces acting on a particle from the adsorbed state (6 nm position) to the middle of the nanopore (0 nm position). According to calculations, the electrostatic force is a few orders of

magnitude larger than the other forces and therefore the primary factor responsible of possible adsorption. The magnitude of the electrostatic force, 14.4 nN, is also considerably higher than the force required to create plastic deformation on a 20 nm polystyrene particle in contact, $\sim 48\text{ pN}$ (see Supporting Information). The strain due to the compressive stress applied on the molecules close to the interface of the particle should be inferred in order to estimate the Raman shift. Unfortunately, rigorous calculations are required, such as combined molecular dynamics and finite element method (FEM) simulations⁴⁷ to further analyse the elastoplastic contacts at the nano-scale. Therefore, currently the full information does not exist regarding the mechanical changes undergone by the nanoparticle and its effect on the Raman spectrum when it is adsorbed.

Conclusions

In conclusion, the goal of this research is to identify a single dielectric nanoparticle. The experiments reported on single nanoparticle SERS detection prior to this report have been performed on random substrates, where the detection area and number of particles cannot be controlled. The first experiments performed for SERS of 20 nm polystyrene nanoparticles were done on similar substrates in order to compare with single particle SERS. After analysing the SERS of the particles, the electric field was localized down to the nanoparticle's scale by using gold-coated nanopores to ensure single particle detection. However, this localization can also cause the particle to rapidly escape the detection area as mentioned before. Therefore, this investigation also considered the optical trapping properties of the nanopore with changing power. It was observed that up to $\sim 10\text{ s}$ of trapping was possible without damaging the particle. It was observed that the single SERS peak at $\sim 785\text{ cm}^{-1}$ was temporally changing position and as the laser power increased, the probability of jumping into a second state at $\sim 815\text{ cm}^{-1}$ increases. This change was related to the adsorption of the particle. The same experiment with different nanopores was conducted multiple times and the reproducibility was approved (see Supporting Information Figure S4). This phenomenon is open to further studies and requires further explanation. Apart from the SERS of nanoparticles we observed that with higher concentration of nanoparticles, it is possible to aggregate the nanoparticles¹¹. It should be noted that the aggregation resulted in bulk Raman spectrum of polystyrene, different than the SERS of nanoparticles.

This research is anticipated to contribute to the label-free detection of nano-bio-particles such as viruses and proteins. Conventional Raman spectroscopy of a solution consisting of different particles would result in an incomprehensible signal of peaks from all particles. Because the platform ensures the detection of a single particle, it is possible to detect a variety of such particles in a mixed solution, one by one⁴⁸. It can also provide information on any change the particle undergoes, which can be used for a variety of research applications such as biological transformations, chemical reactions in nanoscale

and mechanical properties of nanoparticles. Using optical trapping and local detection techniques for measuring the forces acting on the particles in the micro scale is a common technique^{49,50} and it is expected that this work will contribute to that research in the nano-scale.

Methods

Device Fabrication The nanopore wafers were previously fabricated by the 200 mm wafer scale silicon nanocavity array process flow⁵¹ and diced into 21x21 mm samples containing 36 nanopores. The sample was dipped into 1% hydrogen fluoride (HF) solution for 10 minutes and a drop of 49% HF was put on the back-side of the sample for 90 seconds to remove the buried oxide layer. The Si surface was cleaned by RCA-1 cleaning. The width of the nanopore was decreased to 33 nm by sputtering 10 nm Ti adhesion layer and 130 nm Au on top-side of the nanopore.

The size of the nanopores is matched with the size of the nanoparticle studied. It is designed to be just slightly larger than the size of nanoparticles, in order to obtain high SERS signals. Wider pores were tested and resulted in low or no SERS signals. No SERS signals were observed from the pores smaller than nanoparticles because the particles cannot enter into the nanopores. Since 20±5 nm polystyrene beads are used, nanopores are designed at the size of 30 ± 5 nm. The measured size variation of the nanopores is determined by three factors: the size uniformity of Si nanopores, uniformity of gold deposition and measurement errors. First, it should be noticed that a 200 mm CMOS pilot line is used to fabricate the silicon nanopores using deep UV lithography yielding in a high precision. More errors arise from the subsequent Au deposition process. This process was done in the 150 mm research-level lab. The sputtering is not very uniform across the whole chamber. A scanning electron microscope (SEM) is used to check the size of nanopores after each sputtering. The two factors that can influence the reproducibility are: (1) the grain size of the gold deposition is ~ 5 nm, and (2) the resolution of the SEM is 2~3 nm.

The rough gold surface sample was transferred from a rough Ag surface, as Au is a more stable material during measurements and is also the identical material with our nanopores in account of any potential chemical effects contributed to SERS. The Ag surface is prepared by dipping a glass slide into 125 mg/ml of 100 nm Ag nanoparticles in ethanol solution (Blue Nano, Inc., US). After the slide is dried in air, 5 nm Ti and 30 nm Au were sputtered on top to copy the rough surface of Ag particles.

Experimental Setup All experiments were performed with a linearly polarized 785 nm laser and the signal was collected with a Witec α300 Raman setup equipped with an EMCCD. For all experiments with nanoparticles, the nanoparticle solution was ultrasonicated before the experiment to prevent aggregation.

For rough gold surface experiments, the laser (5 mW) was focused on the sample by a 10x (NA 0.25) Zeiss objective. To obtain a smooth spectrum, the signal was averaged over 20

spectra of 10 s integration time. For each experiment, one set of data was taken before and after placing a drop of deionized water (18 MΩ) containing 0.004% w/v 0.02 μm IDC surfactant-free latex beads.

Before each nanopore experiment, the samples were cleaned of contaminants by placing the sample in O₂ plasma chamber for 10 minutes for both sides of the sample. To ensure the full wetting of the sample, right after O₂ plasma, a drop of 1:1 isopropyl alcohol and water solution was spread over it. Upon wetting, the sample was placed in a container only with DI water and the data for background spectrum was collected by focusing 60x water immersion Olympus objective (NA 0.9) with polarization parallel to the short axis of the nanopore, using the laser power at 20 mW. After making sure that the sample was clean by observing no peaks in the spectrum, it was placed in a container with 0.0008% w/v 0.02 μm carboxyl modified (CML) IDC surfactant-free latex beads and the spectrum was collected with 0.3 s integration time, as long as the nanopore was contaminant free as observed from the spectrum. For analysis, ~7 minutes of data was used.

Numerical Calculations In order to estimate the optical enhancement factor of the nanopore and calculate the optical forces acting on the 0.02 μm polystyrene particles, simulations were performed on Lumerical finite-difference time domain (FDTD) software v8.6⁷. All simulations were performed in 3D using the size of the nanopore we obtained by scanning electron microscope (SEM) images. The optical forces were calculated by volumetric optical force analysis provided with the FDTD software.

Acknowledgements

We thank Jos Moonens and Josine Loo for e-beam exposure and Kherim Willems and Maisam Dadgar-Kiani for their valuable discussions. Chang Chen gratefully acknowledges financial support from the FWO (Flanders).

Notes and references

- 1 O. M. Maragò, P. H. Jones, P. G. Gucciardi, G. Volpe and A. C. Ferrari, *Nat. Nanotechnol.*, 2013, **8**, 807–19.
- 2 S. A. Maier, *Plasmonics: Fundamentals and applications*, 2007.
- 3 M. P. Cecchini, A. Wiener, V. Turek, H. Chon, S. Lee, A. P. Ivanov, D. W. McComb, J. Choo, T. Albrecht, S. A. Maier and J. B. Edel, *Nano Lett.*, 2013.
- 4 X.-M. Qian and S. M. Nie, *Chem. Soc. Rev.*, 2008, **37**, 912–920.
- 5 S. Wheaton, R. M. Gelfand and R. Gordon, *Nat. Photonics*, 2014, 8–12.

Journal Name	ARTICLE
6 C. Chen, J. A. Hutchison, P. Van Dorpe, R. Kox, I. De Vlaminck, H. Uji-I, J. Hofkens, L. Lagae, G. Maes and G. Borghs, <i>Small</i> , 2009, 5 , 2876–2882.	24 K. Kneipp, Y. Wang, H. Kneipp, L. T. Perelman, I. Itzkan, R. Dasari and M. S. Feld, <i>Phys. Rev. Lett.</i> , 1997, 78 , 1667–1670.
7 C. Chen, M. L. Juan, Y. Li, G. Maes, G. Borghs, P. Van Dorpe and R. Quidant, <i>Nano Lett.</i> , 2012, 12 , 125–132.	25 C. E. Talley, J. B. Jackson, C. Oubre, N. K. Grady, C. W. Hollars, S. M. Lane, T. R. Huser, P. Nordlander and N. J. Halas, <i>Nano Lett.</i> , 2005, 5 , 1569–1574.
8 C. Chen, J. A. Hutchison, F. Clemente, R. Kox, H. Uji-I, J. Hofkens, L. Lagae, G. Maes, G. Borghs and P. Van Dorpe, <i>Angew. Chemie - Int. Ed.</i> , 2009, 48 , 9932–9935.	26 F. Svedberg, Z. Li, H. Xu and M. Käll, <i>Nano Lett.</i> , 2006, 6 , 2639–2641.
9 M. L. Juan, R. Gordon, Y. Pang, F. Eftekhari and R. Quidant, <i>Nat. Phys.</i> , 2009, 5 , 915–919.	27 J. Prikulis, F. Svedberg, M. Käll, J. Enger, K. Ramser, M. Goksör and D. Hanstorp, <i>Nano Lett.</i> , 2004, 4 , 115–118.
10 Y. Pang and R. Gordon, <i>Nano Lett.</i> , 2011, 11 , 3763–3767.	28 S. M. Asiala and Z. D. Schultz, <i>Chem Commun</i> , 2013, 49 , 4340–4342.
11 A. B. Dahlin, <i>Analyst</i> , 2015.	29 S. M. Asiala and Z. D. Schultz, <i>Anal. Chem.</i> , 2014, 86 , 2625–2632.
12 S. Nam, I. Choi, C.-C. Fu, K. Kim, S. Hong, Y. Choi, A. Zettl and L. P. Lee, <i>Nano Lett.</i> , 2014, 15 , 553–559.	30 J. A. Dieringer, A. D. McFarland, N. C. Shah, D. A. Stuart, A. V. Whitney, C. R. Yonzon, M. A. Young, X. Zhang and R. P. Van Duyne, <i>Faraday Discuss.</i> , 2006, 132 , 9.
13 G. a T. Chansin, R. Mulero, J. Hong, M. J. Kim, A. J. DeMello and J. B. Edel, <i>Nano Lett.</i> , 2007, 7 , 2901–2906.	31 B. Jasse, R. S. Chao and J. L. Koenig, <i>J. Polym. Sci. Polym. Phys. Ed.</i> , 1978, 16 , 2157–2169.
14 M. P. Jonsson and C. Dekker, <i>Nano Lett.</i> , 2013, 13 , 1029–1033.	32 N. E. Marotta and L. A. Bottomley, <i>Appl. Spectrosc.</i> , 2010, 64 , 601–606.
15 H. Im, N. J. Wittenberg, A. Lesuffleur, N. C. Lindquist and S.-H. Oh, <i>Chem. Sci.</i> , 2010, 1 , 688.	33 C. Gullekson, L. Lucas, K. Hewitt and L. Kreplak, <i>Biophys. J.</i> , 2011, 100 , 1837–1845.
16 V. V Thacker, L. O. Herrmann, D. O. Sigle, T. Zhang, T. Liedl, J. J. Baumberg and U. F. Keyser, <i>Nat. Commun.</i> , 2014, 5 , 3448.	34 T. Deckert-Gaudig, E. Rauls and V. Deckert, <i>J. Phys. Chem. C</i> , 2010, 114 , 7412–7420.
17 A. B. Dahlin, M. Mapar, K. Xiong, F. Mazzotta, F. Höök and T. Sannomiya, <i>Adv. Opt. Mater.</i> , 2014, 2 , 556–564.	35 J. R. Anema, a. G. Brolo, a. Felten and C. Bittencourt, <i>J. Raman Spectrosc.</i> , 2010, 41 , 745–751.
18 J. E. Reiner, J. W. F. Robertson, D. L. Burden, L. K. Burden, A. Balijepalli and J. J. Kasianowicz, <i>J. Am. Chem. Soc.</i> , 2013, 135 , 3087–3094.	36 G. Xue, Y. Lu and G. Shi, <i>Polymer (Guildf.)</i> , 1994, 35 , 2488–2494.
19 F. Mazzotta, F. Höök and M. P. Jonsson, <i>Nanotechnology</i> , 2012, 23 , 415304.	37 J. Kim, T. S. Koffas, C. C. Lawrence and G. a. Somorjai, <i>Langmuir</i> , 2004, 20 , 4640–4646.
20 F. Nicoli, D. Verschuere, M. Klein, C. Dekker and M. P. Jonsson, <i>Nano Lett.</i> , 2014, 14 , 6917–6925.	38 H. Nabika, S. Yasuda, H. Ishihara and K. Murakoshi, <i>Nat. Photonics</i> , 2013, 7 , 1–4.
21 C. R. Crick, P. Albella, B. Ng, A. P. Ivanov, T. Roschuk, M. P. Cecchini, F. Bresme, S. A. Maier and J. B. Edel, <i>Faraday Discussions</i> , 2015.	39 J. K. Sass, H. Neff, M. Moskovits and S. Holloway, <i>J. Phys. Chem.</i> , 1981, 85 , 621–623.
22 Y. Li, F. Nicoli, C. Chen, L. Lagae, G. Groeseneken, T. Stakenborg, H. W. Zandbergen, C. Dekker, P. Van Dorpe and M. P. Jonsson, <i>Nano Lett.</i> , 2015, 15 , 776–782.	40 D. V. Chulhai and L. Jensen, <i>J. Phys. Chem. C</i> , 2013, 117 , 19622–19631
23 S. Nie, <i>Science (80-)</i> , 1997, 275 , 1102–1106.	41 J. A. Dieringer, R. B. Lettan, K. A. Scheidt and R. P. Van Duyne, <i>J. Am. Chem. Soc.</i> , 2007, 129 , 16249–16256.

ARTICLE

Journal Name

- 42 W.-H. Park and Z. H. Kim, *Nano Lett.*, 2010, **10**, 4040–4048.
- 43 Y. Rharbi, *Phys. Rev. E*, 2008, **77**.
- 44 H. Liem, J. Cabanillas-Gonzalez, P. Etchegoin and D. D. C. Bradley, *J. Phys. Condens. Matter*, 2004, **16**, 721–728.
- 45 T. A. Yano, Y. Inouye and S. Kawata, *Nano Lett.*, 2006, **6**, 1269–1273.
- 46 Y. Furushima, K. Tazaki and H. Fujimoto, *Solid State Commun.*, 2006, **140**, 240–244.
- 47 H. Eid, G. G. Adams, N. E. McGruer, A. Fortini, S. Buldyrev and D. Srolovitz, *Tribol. Trans.*, 2011, **54**, 920–928.
- 48 N. Arjmandi, W. Van Roy and L. Lagae, *Anal. Chem.*, 2014, **86**, 4637–4641.
- 49 A. R. Clapp and R. B. Dickinson, *Langmuir*, 2001, **17**, 2182–2191.
- 50 E. Schäffet, S. F. Nørrelykke and J. Howard, *Langmuir*, 2007, **23**, 3654–3665.
- 51 K. Malachowski, R. Verbeeck, T. Dupont, C. Chen, Y. Li, S. Musa, T. Stakenborg, D. Sabuncuoglu Tezcan and P. van Dorpe, *ECS Trans.*, 2013, **50**, 413–422.